Journal of Materials Chemistry B

ROYAL SOCIETY OF CHEMISTRY

PAPER

View Article Online
View Journal | View Issue

Cite this: J. Mater. Chem. B, 2021, 9, 3838

A hybrid membrane coating nanodrug system against gastric cancer *via* the VEGFR2/STAT3 signaling pathway†

Ying Long,[a] Zhou Wang,[a] Jialong Fan,[a] Liqin Yuan,[b] Chunyi Tong,[a] Yanzhong Zhao*[c] and Bin Liu*[a]

Although drug combination has proved to be an efficient strategy for clinic gastric cancer therapy, how to further improve their bioavailability and reduce the side effects are still challenges due to the low solubility and untargeted ability of drugs. Recently, newly emerging nanotechnology has provided an alternative for constructing new drug delivery systems with high targeting ability and solubility. In this study, a pH-responsive liposome (Liposome-PEO, LP) loaded with apatinib (AP) and cinobufagin (CS-1) was used for combinational therapy against gastric cancer after coating with a hybrid membrane (R/C). The results indicated that the constructed nanocomplex LP-R/C@AC not only efficiently killed tumor cells *in vitro* by inducing apoptosis, autophagy, and pyroptosis, but also significantly inhibited tumor invasion and metastasis *via* the VEGFR2/STAT3 pathway. Moreover, it showed stronger anti-tumor activity in gastric cancer-bearing mouse models, as compared to the sole drugs. A naturally-derived hybrid cell membrane coating bestowed nanocomplexes with enhanced biointerfacing including prolonged circulation time and targeting ability.

Received 6th January 2021,
Accepted 5th April 2021

DOI: 10.1039/d1tb00029b

rsc.li/materials-b

Introduction

As a serious disease with high incidence, gastric cancer ranks third in mortality among all tumors. At present, the commonly used strategy that combines surgery and chemotherapy has made progress in improving the quality of life and delaying the development of this disease.[1] However, the non-selective application of drugs to various types of patients leads to limited therapeutic effects, multi-drug resistance, and strong toxic and side effects.[2] By classifying the molecular characteristics of gastric cancer, we found that the vascular endothelial growth factor (VEGF) acts as an important carcinogenic gene in many gastric cancer patients.[3] Mounting evidence has indicated that the abnormal activation of the VEGF/VEGFR2 pathway can not only promote the generation of new blood vessels, but also accelerate the cell proliferation and migration, induce the exacerbation of vascular permeability, intensify tumor microenvironment hypoxia and acidosis, significantly inhibit the tumor immune function, and promote malignant development on multiple levels.[4,5] As the downstream target molecule of VEGFR2, STAT3 in cancer cells immediately regulates the expression of numerous oncogenes including VEGF after continuous activation. In turn, VEGF can activate STAT3 signaling to produce a signal feed forward loop in cancer cells.[6] Therefore, the inhibition of VEGFR2 has been recognized as an important anticancer strategy.

As a small molecule inhibitor against VEGFR2, apatinib exerts its strong anti-angiogenesis function by inhibiting phosphorylation by specifically targeting the intracellular kinase ATP binding site.[7] Although the drug with approval from the China Food and Drug Administration (CFDA) showed a good safety profile and the ability to significantly extend the overall survival of advanced gastric cancer patients with multi-drug resistance,[8] the bioavailability of the simple oral administration of apatinib was poor, with more than 59.0% of the drug being directly excreted from the stool after administration. Therefore, in order to achieve certain therapeutic effects, a high dose (750–850 mg d^{-1}) is usually required, which often causes hypertension, proteinuria and hand-foot syndrome in patients.[9]

Cinobufagin (CS-1) is a toad diene hydroxy acid lactone compound with good anti-tumor and anti-inflammatory activity. Studies have shown that it can mediate a highly effective anticancer effect by targeting several important signal pathways of the tumor. For example, it can inhibit tumorigenesis,

[a] College of Biology, Hunan University, Changsha, 410082, China. E-mail: binliu2001@hotmail.com; Fax: +86-731-89720939; Tel: +86-731-89720939
[b] Department of General Surgery, The Second Xiangya Hospital, Central South University, Changsha, 410011, China
[c] Department of Health Management, The Third Xiangya Hospital, Central South University, Changsha, 410011, China. E-mail: yanzhongzhao@163.com

† Electronic supplementary information (ESI) available. See DOI: 10.1039/d1tb00029b

angiogenesis, invasion and metastasis of tumors by blocking the IL-6/STAT3, PI3K/Akt and MAPK pathways;[10–12] it can inhibit tumor proliferation by inducing cell cycle arrest at the G2/M stage through the GSK-3/NF-κB signaling pathway;[13] it was also reported to exert immunomodulatory effects on peritoneal macrophages.[14] Therefore, it is reasonable to suspect that the combination of CS-1 with AP can not only repress the VEGF expression, but also inhibit the growth, invasion and metastasis of tumors through different signaling pathways. However, considering the disadvantages of AP and CS-1 such as poor water solubility, short half-life *in vivo* and low bioavailability, it is urgent to change their dosage form.

Compared with traditional drug carriers, nano-drug carriers have many unique advantages. By utilizing the high permeability and retention (EPR effect) characteristic of blood vessels and tumor tissues, nanoparticles can permeate and accumulate in the blood vessels at tumor sites. Moreover, a variety of specific targeted molecules can be modified on the surface of nano-carriers, which helps target tumor sites more effectively. In addition, modifications can be adjusted according to the application requirements to increase the carrier's half-life and control drug release, so as to reduce the dose and side effects of drug administration without affecting the anti-tumor efficiency.[15] Until now, several nanomedicines such as liposomal Active Ingredient have been used for clinical tumor therapy and many are in the pipeline of clinical trials.[16]

Recently, inert polymer molecules such as polyethylene glycol (PEG) coating on the liposomes have extended the circulation time of the drug delivery system in the blood so that the amount of drugs accordingly increased in the tumor tissue. Meanwhile, the stereo-hindrance effect provided by the hydrophilic polymer improves its surface performance and prevents the modified liposomes from being trapped and quickly swept away by the reticuloendothelial system (RES).[16] The pH-sensitive lipid DSPE-PEOz could also accelerate drug release under acidic environments.[17] Although great achievements have been made for long-circulation liposomes, there are still some defects, such as the phenomenon of the "accelerated blood clearance rate" (ABC), low cell uptake and poor selectivity to cancer cells.[16] To this end, researchers have skillfully utilized membrane structures to endow nanomaterials with new properties.[18] For example, red blood cell membrane (RBC) coating could stably resist the clearance mechanism of NPs in the body to extend the systemic circulation half-life.[19,20] Recently, nanoparticles coated with cancer cell membranes (CCM) showed the enhanced enrichment of drugs in tumor sites due to the homotypic adhesion properties for active targeting.[21] Therefore, nanoparticles coated with erythrocyte and cancer cell hybrid membranes can simultaneously extend the half-life and improve the targeting ability of drugs to tumor sites.[22]

To improve the bioavailability and reduce the side effects of drugs, we have proposed pH-responsive liposome (Liposome-PEO) nanoparticles as a drug carrier to co-deliver the two poorly water-soluble drugs of AP and CS-1 (LP@AC), which can precisely target gastric cancer. Nanoparticles were further coated with the hybrid membrane (R/C) originating from red blood cells (RBC) and cancer cells (CCM) to obtain the final nanomaterial LP-R/C@AC (Scheme 1). Our data has shown that this kind of nanomedicine loading with dual drugs possesses the advantages of pH-responsiveness, high biocompatibility, tumor-targeted accumulation and immune escape ability, which can confer tumor inhibition efficiency with low drug dosage and side effects. Therefore, the newly developed nanodrug complex has demonstrated a possible clinical application for the treatment of advanced gastric cancer.

Experimental

Materials

Apatinib (AP) was purchased from Selleck (TX, USA). Cinobufagin (CS-1) was obtained from Herbest (Xi'an, China). DSPE-PEOz2K was purchased from Xi'an RuiXi Biological Technology Co. Ltd (Xi'an, China). Polysorbate-20 (Tween-20), 1-ethyl-3-(3-dimethylaminopropyl) carbodiimide (EDC), *N*-hydroxy-succinimide (NHS), 4′,6-diamidino-2-phenylindole (DAPI) and dimethyl sulfoxide (DMSO) were obtained from Sigma-Aldrich (MO, USA). Hoechst 33342 was obtained from Yeasen (Shanghai, China). DiI (1,1′-dioctadecyl-3,3,3′,3′-tetramethylindocarbocyanine perchlorate, DiIC18(3)) and DiO (3,3′-dioctadecyloxacarbocyanine perchlorate, DiOC18(3)) were purchased from Beyotime (Shanghai, China). Cy5.5 NIR fluorescence dye was obtained from Solarbio (Beijing, China). Protease and phosphatase cocktail inhibitors were purchased from Abmole (TX, USA). Lecithin and cholesterol were obtained from Shanghai Ryon Biological Technology Co. Ltd (Shanghai, China). CCK-8 was obtained from TargetMol (MA, USA). Hematoxylin–eosin staining kit was obtained from Solarbio (Beijing, China). DeadEnd™ Fluorometric TUNEL System was purchased from Promega Corporation (WI, USA). Roswell Park Memorial Institute 1640 (RPMI1640), Dulbecco's Modified Eagle Medium (DMEM) and phosphate buffer saline (PBS) were obtained from HyClone (UT, USA). Active Ingredient–Active Ingredient (PS) was obtained from Invitrogen (CA, USA). Fetal bovine serum (FBS) was obtained from Gibco (PA, USA). ROS kit and calcein-AM/PI were purchased from Yeasen (Shanghai, China). A cell cycle detection kit was purchased from Beyotime (Shanghai, China). Annexin V Cell Apoptosis Analysis Kit was purchased from Tianjin Sungene Biotech Co. Ltd (Tianjin, China). Regular range prestained protein marker (PL00001) and extra range prestained protein marker (PL00003) were purchased from Proteintech (IL, UAS). Active Ingredient was purchased from Beyotime (Shanghai, China). Chloroquine and methyl-β-cyclodextrin were obtained from Sigma-Aldrich (MO, USA). LysoTracker Green DND-26 was purchased from Yeasen (Shanghai, China). All chemicals were at least reagent grade.

Antibodies: p-NF-κB p65 (Ser536), p-STAT3 (Tyr705), p-VEGFR2 (Tyr1175), VEGFR2 and LC3A/B were obtained from Cell Signaling Technology (MA, USA). Cyclin D1, DFNA5/GSDME, NF-κB p65, MMP-9, PD-L1, CD44, Mcl-1, GAPDH, HRP-conjugated Affinipure Goat Anti-Mouse IgG (H + L) and HRP-conjugated Affinipure Goat Anti-Rabbit IgG (H + L) were purchased from Proteintech (IL, UAS). CD47 and HIF-1α were obtained from Bioss (Beijing, China).

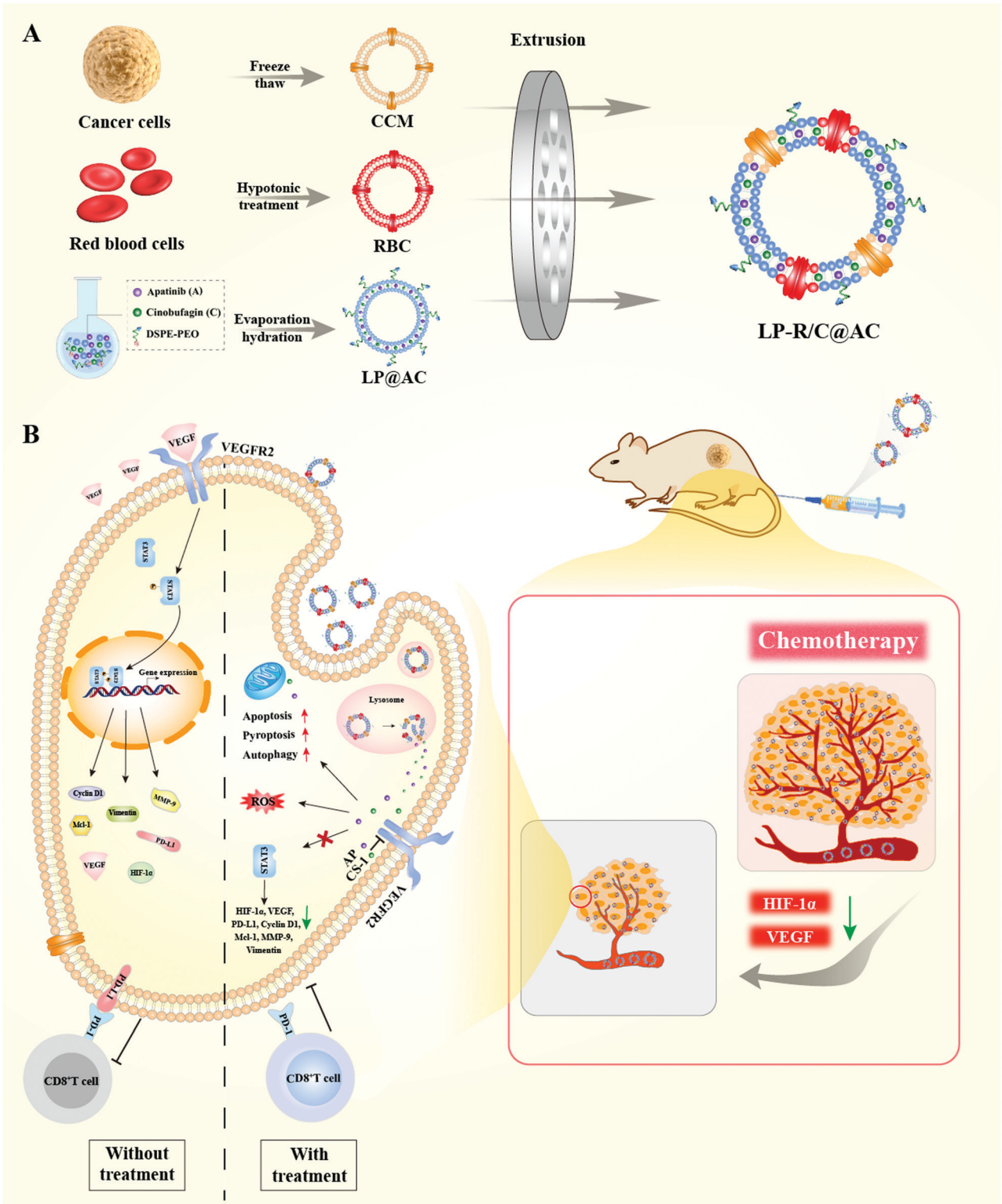

Scheme 1 (A) Preparation scheme of hybrid membrane-modified dual drug nanocarrier system (LP-R/C@AC NPs). (B) Proposed mechanism of LP-R/C@AC NPs mediated antitumor efficacy.

Caspase-3 was obtained from Bimake (TX, USA). VEGF, Vimentin, Alexa Fluor 488-labeled Goat Anti-Mouse IgG (H + L) and Alexa Fluor 488-labeled Goat Anti-Rabbit IgG (H + L) were purchased from Beyotime (Shanghai, China).

Cell lines and animals

HGC-27 (human gastric cancer cell line), RAW264.7 (mouse macrophage cell line), HUVEC (human umbilical vein endothelial cell line) and SMC (human smooth muscle cell line) were

provided by the Cell Library of Xiangya Central Laboratory, Central-South University. All kinds of cells were cultured in RPMI1640 or DMEM with 10% (v/v) FBS and 1% Active Ingredient & Active Ingredient with 5% CO_2 at 37 °C. BALB/c mice and BALB/c nude mice at 4–5 weeks old were purchased from Hunan SJA Laboratory Animal Co. Ltd. All animal experiments complied with the guiding principles of the "Declaration of Helsinki, DoH" and were ratified by the Medical Ethics Committee of Xiangya Third Hospital of Central South University.

Preparation of RBC membrane, HGC-27 membrane, and hybrid membrane

The red cell membranes were prepared according to our previously established protocol.[20] In short, the collected fresh whole blood (~2 mL) from BALB/c mice was suspended in 5 mL of Active Ingredient-containing PBS solution and centrifuged at 4 °C, 3500 rpm for 10 min; the supernatant was discarded. Next, 10 mL of hypotonic solution was added to the precipitate and incubated at 4 °C for 2 h. Afterward, the red cell lysate was centrifuged at 4 °C, 12 000 rpm for 10 min, and re-suspended with 4 °C pre-cooling PBS until the supernatant liquor turned colorless. The red blood cell membranes (RBC) obtained through centrifugation were refrigerated at −80 °C for further use.

The HGC-27 cell membranes were prepared in accordance with the instructions of the cell membrane protein and cytoplasmic protein extraction kit (Beyotime, China). In short, cultured HGC-27 cells were scraped off from dishes after washing with pre-cooling PBS and centrifuged at 1000 rpm for 5 min. The obtained cellular debris was treated as described above. Then, membrane protein extraction reagent A with protease inhibitor was added to the cellular debris and the mixture was further incubated for 15 min on ice. After freeze–thaw and sonication for 3 cycles, the mixture was centrifuged at 800 rpm for 10 min to collect the supernatant. Finally, the resulting precipitate of the cancer cell membrane (CCM) was obtained from the supernatant through centrifugation at 13 000 rpm for 30 min.

A BCA protein assay kit (Solarbio, China) was employed to quantify the protein concentration of HGC-27 and RBC membranes. The two kinds of HGC-27 and RBC membranes were mixed with the same protein weight. The mixture was then stirred at 37 °C for 3 h *via* sonication treatment (50 w/5 min) to prepare a hybrid membrane (R/C). Finally, the products were extruded *via* a HandExtruder (Genizer LLC, USA) to obtain uniform particles.

Synthesis of LP-R/C@AC NPs

The pH-responsive nanodrug complex based on liposome nanoparticles (Liposome-PEO-AP-CS-1, LP@AC) was synthesized according to a previous study.[17] Lecithin, cholesterol, DSPE-PEOz, AP and CS-1 (molar ratio of 2 : 1 : 0.4 : 2 : 0.006–0.05) were dissolved in 3 mL of chloroform. The mixture, after ultrasonic treatment for 5 min, was transferred into a round-bottom flask to evaporate the chloroform under low pressure. The formed transparent thin film was hydrated with 3 mL PBS and emulsified for 1 h under rotation. The liposome-PEO-AP-CS-1 (LP@AC) product was sonicated before they extrusion through a liposome HandExtruder (Genizer LLC, USA) with different pore size filters. Next, the LP@AC was mixed with the hybrid membrane (R/C) with a 5 : 1 phospholipid ratio and stirred at 37 °C for 3 h. After the mixture was extruded through the HandExtruder, the obtained uniform LP-R/C@AC NPs was used for the subsequent experiments (the nano-drug complex containing AP or CS-1 alone was synthesized using a similar method).

Abbreviations for different nanomaterials in this article: LP: liposome-PEO; LP-R: liposome-PEO-RBC; LP@AC: liposome-PEO-AP-CS-1; LP-R/C: liposome-PEO-R/C; LP-R/C@A: liposome-PEO-AP-R/C; LP-R/C@C: liposome-PEO-CS-1-R/C; LP-R/C@AC: liposome-PEO-AP-CS-1-R/C.

Characterization of LP-R/C@AC NPs

Zeta-potential and size distribution of the samples in PBS were measured by a ZetaSizer Nano series Nano-ZS (Malvern Nano Series, UK). The morphology of LP-R/C@AC NPs at different pH buffer solutions was detected by a transmission electron microscope (TEM) (JEOL, Japan).

Membrane fusion assay was carried out according to the previous study.[22] Briefly, CCM and RBC membrane were stained with DiO (green fluorescence) and DiI (red fluorescence), respectively. After stirring in the dark for 30 min, the separate membrane solutions were centrifuged with 13 000 rpm for 30 min to remove the free dye. The membrane mixture was then treated with sonication for 3 min followed by stirring in the dark for 3 h to complete the membrane fusion process. The fusion of LP@AC (DiO) and R/C (DiI) was performed with the above procedure. Confocal laser scanning microscopy (CLSM) (FV1200, Olympus, Japan) was employed to study membrane colocalization.

Förster resonance energy transfer (FRET) study was employed to further study the membrane fusion. The HGC-27 cell membrane was labeled with a pair of FRET fluorochromes, DiI ($\lambda_{ex}/\lambda_{em}$ = 549/565 nm) and DiD ($\lambda_{ex}/\lambda_{em}$ = 644/663 nm). The RBC membrane was then mixed with the fluorochrome-labeled HGC-27 membrane at weight ratios of 0 : 1, 1 : 1, 3 : 1 and 5 : 1, respectively. The mixture was stirred in the dark for 3 h, after sonication treatment for 5 min. The fluorescence spectra were recorded between 550 and 750 nm by an FL-2500 fluorescence spectrophotometer (Hitachi, Japan) with an excitation wavelength of 525 nm.

SDS-PAGE and Western blot (WB) were employed to characterize the membrane proteins. RBC, HGC-27 cell membrane (CCM), hybrid membrane (R/C) and LP-R/C@AC nanocomplex were extracted using the membrane protein extraction reagent B (Beyotime, China) based on the kit instructions. Protein samples were mixed with loading buffer (Beyotime, China) and denatured at 95 °C for 5 min. Afterwards, samples (20 μg) were separated by 10% SDS-PAGE gel. The proteins transferred to the PVDF membrane were blocked using 5% nonfat milk for 1 h. After washing 3 times with TBST for 5 min, the membrane was incubated with diluted primary antibodies such as anti-CD44, anti-CD47 at 4 °C overnight, and the PVDF

membrane was incubated with HRP-conjugated secondary antibody for 1 h at room temperature. After washing with TBST 3 times for 5 min, the PVDF membrane was subjected to Supersignal™ West Pico Plus chemiluminescent substrate (ThermoFisher, USA), and the signals were captured by a BIO-RAD ChemiDoc XRS chemiluminescence system (Bio-Rad, USA). Another corresponding SDS-PAGE gel was stained with Coomassie Blue for 2 h and decolored overnight for subsequent imaging.

Controlled drug release from LP-R/C@AC NPs *in vitro*

Next, we investigated the release characteristics of AP and CS-1 from LP-R/C@A and LP-R/C@C NPs at different pH values (pH 5.2 and pH 7.4) by recording the AP and CS-1 amount at different time points (2, 4, 6, 8, 12, 24, 36, 48, 60 and 72 h). All the formulations with equivalent loaded AP or CS-1 dose (1 mg mL^{-1}, 2 mL) were enclosed in a dialysis bag (2.5 kDa) and immersed in 50 mL PBS solution with different pH values and stirred in a 37 °C water bath. The amounts of AP and CS-1 in different solutions at each time point were detected by HPLC (Agilent 1260 liquid chromatography, USA). The entrapment efficiency of AP and CS-1 were calculated based on the following equation:

$$\text{Entrapment efficiency } (\%) = \frac{M_T - M_U}{M_T} \times 100\%$$

In this equation, M_U represents the mass of the unencapsulated drug, and M_T represents the total mass of the drug.

Biocompatibility analysis

Cell cytotoxicity assay: The cytotoxicity of LP-R/C NPs on SMC cells, HUVEC and HGC-27 cells were detected using Cell Counting Kit-8 (CCK-8). In short, cells seeded in the 96-well plate (5×10^3 cells per well) were cultivated for 24 h. After that, the cells were treated with different concentrations of LP-R/C NPs (0, 15, 30, and 60 μg mL^{-1}) for 24 h and an appropriate quantity of CCK-8 was added to the culture medium. After incubation at 37 °C for 1 to 4 h, the absorbance values of cells at 450 nm were read by a PerkinElmer microplate reader (EnSpire 2300, Singapore). Cell viability was calculated according to the following equation:

$$\text{Cell viability}(\%) = \frac{OD_{450nm(sample)}}{OD_{450nm(control)}} \times 100\%$$

Hemolysis assay: Erythrocytes of BALB/c mice were collected, washed with PBS and gathered through centrifugation at 3500 rpm for 5 min. Then, a 4% red cell suspension (v/v, in PBS) was blended with different concentrations of AP, CS-1, AC, LP@AC and LP-R/C@AC NPs (0, 30, 60, and 120 μg mL^{-1}, drug concentration; for AC, LP@AC and LP-R/C@AC group, it mainly represented the concentration of AP). After incubating the mixture at 37 °C for 4 h, all samples were centrifuged at 3500 rpm, 4 °C, for 5 min to collect the supernatant and measure its absorbance value at 562 nm by a PerkinElmer microplate reader. The hemolysis rate was calculated according to the following equation:

$$\text{Hemolysis } (\%) = \left(\frac{h}{h_0}\right) \times 100\%$$

where h represents the supernatant absorbance value of erythrocytes with different concentrations of AP, CS-1, AC, LP@AC and LP-R/C@AC NPs, while h_0 represents the value of erythrocytes in the pure water.

Platelet aggregation assay: In short, platelet-rich plasma was obtained from the whole blood of BALB/c mice with anticoagulants. Different formulations (AP, CS-1, AC, LP@AC and LP-R/C@AC) with a drug concentration of 100 μg mL^{-1} were gently added to the plasma and incubated at room temperature for 1 h. The absorbance values of cells at 650 nm were measured by a microplate reader. Platelet-rich plasma samples mixed with PBS or thrombin were used as negative and positive controls, respectively. The ratio of plasma : sample was 9 : 1 (v/v) in a 50 μL system. The turbidity rate was calculated as follows:

$$\text{Turbidity } (\%) = \left(\frac{t}{t_0}\right) \times 100\%$$

where t represents the absorbance value of AP, CS-1, AC, LP@AC and LP-R/C@AC at a drug concentration of 100 μg mL^{-1}, and t_0 represents the value of the negative controls.

Anticancer activity of LP-R/C@AC NPs *in vitro*

ROS assay: The HGC-27 cells seeded into 12-well plates (5×10^4 cells per well) were cultured at 37 °C for 24 h. Then, cells were treated with LP-R/C, LP-R/C@A, LP-R/C@C and LP-R/C@AC with the same AP/CS-1 concentration (10/0.03 μM) for 24 h. A ROS kit was employed to stain the cells for 30 min before the images were captured using CLSM.

Cell live/dead staining assay: The HGC-27 cells suspension was seeded into 12-well plates (5×10^4 cells per well) and cultured with 5% CO_2 at 37 °C for 24 h. Next, the wells were added with LP-R/C, LP-R/C@A, LP-R/C@C and LP-R/C@AC at the same AP/CS-1 concentration (10/0.03 μM). After culturing for 24 h, Calcein AM/Propidium Iodide (PI) was employed to stain the cells for 5 min, respectively and the images were captured by CLSM.

Apoptosis assay: The HGC-27 cells suspension was seeded into 6-well plates (1×10^5 cells per well) and cultivated for 24 h. Next, LP-R/C@A, LP-R/C@C and LP-R/C@AC were added to the cells with the same AP/CS-1 concentration (10/0.03 μM) and treated for 24 h. The Annexin V-FITC/PI Apoptosis Detection Kit was employed to stain the cells, and flow cytometry (CytoFLEX, Beckman, USA) was used to measure the cell apoptosis rate.

Cell cycle analysis: The HGC-27 cells suspension was seeded into 6-well plates (1×10^5 cells per well) and cultivated for 24 h. Next, LP-R/C@A, LP-R/C@C and LP-R/C@AC were added into cells with the same AP/CS-1 concentration (10/0.03 μM), and treated for 24 h. Then, harvested cells were fixed with 70% (v/v) ethanol for 24 h. A cell cycle detection kit was used to stain cells for cell cycle analysis by flow cytometry (Athena, Cytek, CA, USA). The data were analyzed by Modfit software.

Western blot: The HGC-27 cells suspension was seeded into 6-well plates (1×10^5 cells per well) and cultured for 24 h. Then, LP-R/C@A, LP-R/C@C and LP-R/C@AC were added to the cells with the same AP/CS-1 concentration (10/0.03 μM).

After culturing for 48 h, the collected cells were lysed using RIPA buffer for WB assay as described above.

Assay of migration and invasion

Scratch wound healing assay: The HGC-27 cells suspension was seeded into 12-well plates (5×10^4 cells per well) and cultured until the monolayer cells grew to full confluence. A 100 μL sterile pipette tip was used to scratch cells and the detached cells were removed by washing with PBS. LP-R/C@A, LP-R/C@C and LP-R/C@AC NPs were added to the wells with a serum-free medium at the same AP/CS-1 concentration (10/0.03 μM). After 48 h, the images of the wound area were photographed under an inverted microscope (TI-S, Nikon, Japan).

Immunofluorescence assay: The cultured HGC-27 cells in confocal dishes were treated with LP-R/C@A, LP-R/C@C and LP-R/C@AC NPs at the same AP/CS-1 concentration (10/0.03 μM) for 48 h. Then, the cells were sequentially fixed with 4% paraformaldehyde and permeabilized with 0.3% TritonX-100 for 10 min. After blocking with 10% goat serum for 1 h, the cells were incubated with primary antibodies (1 : 200, 10% goat serum, in PBST) against Vimentin (overnight at 4°) and Alexa Fluor 488-conjugated secondary antibodies (1 : 500, PBST) in the dark for 1 h at room temperature. Meanwhile, cell nuclei were stained with DAPI for 20 min before imaging under CLSM.

Immune escape, tumor targeting and pharmacokinetics of LP-R/C@AC NPs

Macrophage phagocytosis assay: The immune escape ability of LP, LP-R and LP-R/C NPs was tested using RAW264.7 cells. Briefly, after culturing macrophages RAW264.7 (5×10^4 cells per well) for 24 h, DiI-labeled nanoparticles (LP-DiI, LP-R-DiI and LP-R/C-DiI, 25 μg mL^{-1}) were added to macrophages for 4 h. DAPI was used to stain nuclei for 20 min in the dark. After washing 3 times with warm PBS, the cell images were captured through CLSM.

Cellular uptake assay: The HGC-27 cells suspension seeded into confocal dishes were cultured for 24 h. Then, cells were treated with DiI-labeled nanoparticles (LP-DiI, LP-R-DiI and LP-R/C-DiI, 50 μg mL^{-1}) for 3 h. DAPI was used to stain the cell nuclei for 20 min in the dark. Cell images were captured using CLSM.

The cellular uptake mechanism assay of LP-R/C NPs: The HGC-27 cell suspension seeded into confocal dishes was cultured for 24 h. The cells were then treated with DiI-labeled nanoparticles (LP-R/C-DiI, 40 μg mL^{-1}) for 3 h before incubating with different inhibitors such as chloroquine (10 μM), Active Ingredient (10 μM), and methyl-β-cyclodextrin (20 μM) for 1 h. Next, DAPI was used to stain the cell nuclei for 20 min in the dark. Cell images were captured using CLSM.

Lysosomal staining: The HGC-27 cell suspension seeded into confocal dishes was cultured for 24 h, then the cells were treated with DiI-labeled nanoparticles (LP-R/C-DiI, 50 μg mL^{-1}) for 3 h. Next, a lysosomal probe (LysoTracker Green DND-26, at a final concentration of 75 nM) was used to stain the lysosome for 30 min. Subsequently, DAPI was used to stain the cell nuclei for 20 min in the dark. Cell images were captured using CLSM.

Pharmacokinetics assay: Cy5.5, LP-Cy5.5, and LP-R/C-Cy5.5 NPs with equivalent amounts of Cy5.5 (0.1 mg kg^{-1}) were intravenously injected into BALB/c mice. At different time points (0, 1, 2, 3, 4, 6, 12, and 24 h), 100 μL blood samples were collected and centrifugated at 3500 rpm for 5 min. An IVIS kinetics optical system (PerkinElmer, CA) was used for the fluorescence imaging visualization of the supernatant. A fluorescence spectrophotometer (FL-2500, Japan) was used to quantify the fluorescence intensity of the serum. SigmaPlot 12.0 software was used to fit the obtained data and calculate the final result.

Tumor targeting and biodistribution assay: The animal model was built by subcutaneously injecting 1×10^7 HGC-27 cells (150 μL) on the back of BALB/c nude mice. When the tumor volume reached about 200 mm^3, 150 μL of Cy5.5, LP-Cy5.5 and LP-R/C-Cy5.5 NPs with an equivalent amount of Cy5.5 (0.1 mg kg^{-1}) were respectively administered intravenously to the mice. At 0, 12, 24, 36, and 48 h after administration, fluorescence images were obtained with the IVIS kinetics optical system. The mice were sacrificed at 48 h to collect the tumor tissues and major organs (heart, liver, spleen, lung, and kidney). The fluorescence intensities of these organs were obtained from the corresponding fluorescence images.

In vivo antitumor activity assay and safety evaluation

HGC-27 tumor-bearing nude BALB/c mice established as described above were randomly divided into 6 groups (n = 5 per group). When the tumor volume reached about 100 mm^3, PBS, AP, CS-1, AC, LP@AC and LP-R/C@AC NPs (AP 7.5 mg kg^{-1}, CS-1 0.2 mg kg^{-1}) were intravenously injected at 2 day intervals for 16 days. The first day of injection was designated as day 0. Body weight and tumor volumes (TV) were recorded every 2 days, and the TV was calculated according to the formulation:

$$\mathrm{TV}\ (\mathrm{mm}^3) = \frac{1}{2}(L \times W^2)$$

where L and W represent the length and width of the tumor, respectively.

The tumor inhibition rate (TIR) was calculated as follows:

$$\mathrm{TIR}\ (\%) = \frac{(\mathrm{TV} - \mathrm{TV}_t)}{\mathrm{TV}} \times 100\%$$

where TV represents the average volume of tumors in the control (PBS) group and TV_t represents the average volume of tumors in drug-treated groups.

After performing morphological observations, we sacrificed these mice and collected tumor tissues and major organs (heart, liver, spleen, lung, and kidney). Tissues were fixed with 4% paraformaldehyde for 24 h. Next, tissues were embedded in paraffin and cut into sections with a thickness of 5 μm. Histological changes in tumors and major organs were detected by H&E staining, cell apoptosis of tumor tissues was evaluated by TUNEL assay, and the expression levels of PD-L1 and MMP-9 in tumor samples were detected by immunofluorescence assay, all of these experiments were performed according to the standard instructions. Moreover, blood samples of each group were collected for biochemical and hematological assays.

Statistical analysis

Statistical significance was determined by one-way ANOVA and a two-tailed Student's *t*-test using the Prism 8.0 software. The data were the means ± SD; $*p < 0.05$, $**p < 0.01$, $***p < 0.001$.

Results and discussion

Evaluation of the combined effect of AP and CS-1 on anti-proliferative activity

Apatinib (Fig. 1A) is a tyrosine kinase inhibitor that can inhibit the proliferation, metastasis, invasion, and angiogenesis of cancer cells by binding to the ATP site of the catalytic domain of VEGFR2.[7] Molecular docking indicated that both AP and CS-1 could interact with Lys 868, an important residue for maintaining physiological function of VEGFR2.[23] It is interesting to note that except for Lys 868, CS-1 can interact with two other amino acids (Val 914, Val 916) (Fig. S1, ESI†). According to the docking score, CS-1 showed stronger interactions with VEGFR2 as compared with AP (docking score: −24.51 *vs.* −22.15). We suspect that the combination of drugs can improve the efficiency against gastric cancer in theory. Just as we expected, by investigating the IC_{50} value of the two drugs, we found that the IC_{50} values of AP and CS-1 alone for HGC-27 cells were 17.34 μM and 39.38 nM, respectively (Fig. 1B). Then, we tested different ratios of AP/CS-1 to obtain the optimal quantities for the drug combination and found that the cell viability of the HGC-27 cells was about 27% in the presence of 10 μM AP and 30 nM CS-1 (Fig. 1C). The drug dosage decreased by 42.33% and 23.82% as compared with the single IC_{50} value of AP and CS-1, while the killing effect on HGC-27 cells increased 3.48-fold and 1.84-fold as compared with the corresponding concentration of AP or CS-1 alone ($p < 0.0001$). These data indicated that the combination of AP and CS-1 could achieve high efficiency against gastric cancer.

Characterization of the LP-R/C@AC NPs

To improve the bioavailability of AP and CS-1, we constructed a pH-responsive nano-drug carrier system based on liposomes to load these drugs. HPLC assay showed that the entrapment efficiencies of AP and CS-1 in LP-R/C@AC NPs were 94.2% and 99.9%, respectively (Fig. S2, ESI†). Dynamic light scattering (DLS) results for LP-R/C@AC NPs showed uniform size with an average diameter of about 108 nm (Fig. 2A). Meanwhile, the surface charge of LP-R/C@AC NPs was quite close to that of purified R/C membranes (−7.5 mV *vs.* −8.01 mV, Fig. 2B).

Fluorescence imaging was used to demonstrate the successful fusion of the two kinds of membrane. The RBC membrane labeled with DiI and the HGC-27 cell membrane labeled with DiO were mixed to yield the RBC-CCM hybrid membrane. Secondly, LP@AC labeled with DiO and the RBC-CCM (R/C) hybrid membrane labeled with DiI were mixed to form LP-R/C@AC NPs. Fig. 2C indicated a significant colocation of the two different fluorescence signals after membrane fusion, which directly reflected the successful fusion of the two types of natural cell membranes and incorporation with LP@AC to form the hybrid LP-RC@AC NPs. Besides, we employed Förster resonance energy transfer (FRET) assay to monitor the hybrid membrane fusion process. It was found that the fluorescence signal of the donor (DiI) was efficiently quenched by DiO in the sole cancer cell membrane due to the FRET effect. However, the

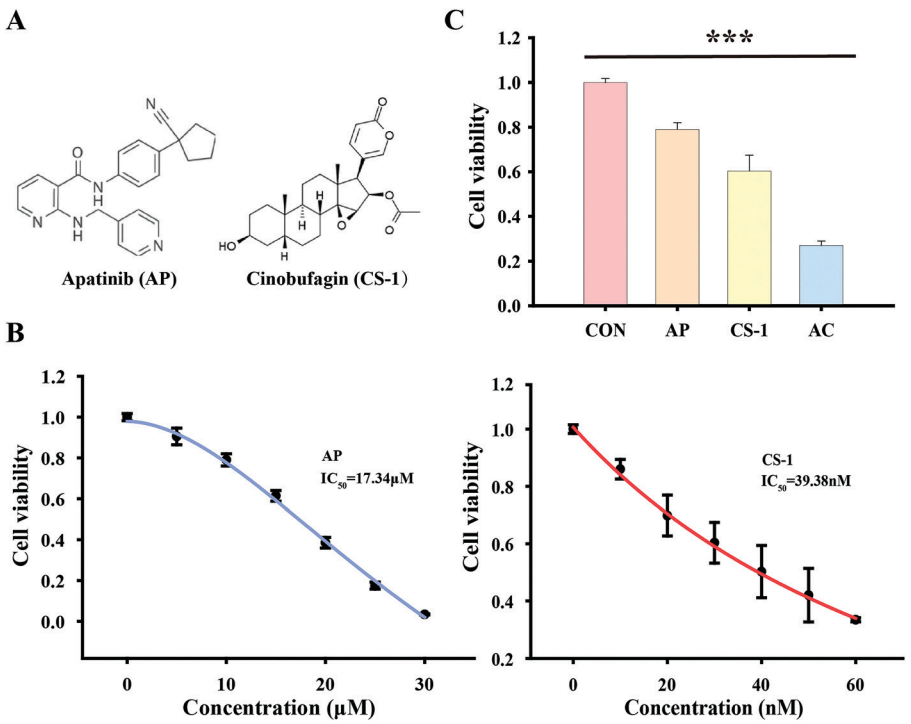

Fig. 1 The effect of drug combination on gastric cancer cell killing. (A) Chemical structure of apatinib (AP) and cinobufagin (CS-1). (B) IC_{50} of AP and CS-1 on HGC-27 cells for 24 h. (C) Optimized ratios of AP (10 μM) and CS-1 (30 nM) against HGC-27 cells; $n = 3$.

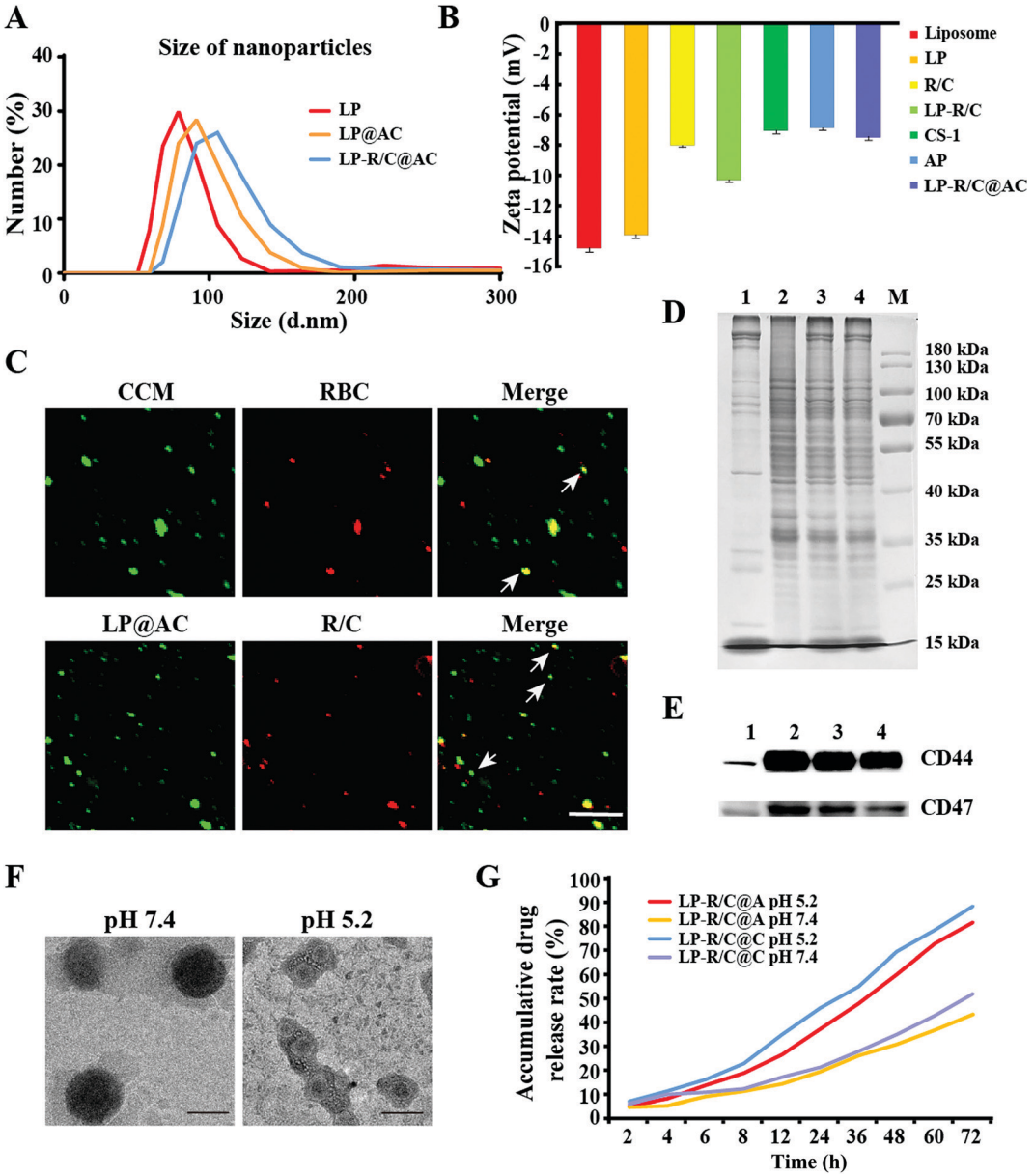

Fig. 2 Characterization of the LP-R/C@AC NPs. (A) Size distribution of LP (81.04 nm, PDI: 0.304), LP@AC (94.62 nm, PDI: 0.358) and LP-R/C@AC NPs (107.90 nm, PDI: 0.395). (B) Zeta potential of different nanomaterials (liposome −14.8 mV, LP −13.9 mV, R/C −8.01 mV, LP-R/C −10.3 mV, CS-1 −7.05 mV, AP −6.85 mV, LP-R/C@AC −7.5 mV). (C) Membrane fusion of hybrid membranes detected by CLSM. The RBC and RBC-CCM (R/C) were labeled with DiI (red), while CCM and LP@AC were labeled with DiO (green), scale bar: 5 μm. (D) SDS-PAGE analysis. 1. RBC, 2. CCM, 3. R/C, 4. LP-R/C@AC, M. marker. (E) Western blot analysis of characteristic markers of different membrane proteins: 1. RBC, 2. CCM, 3. R/C, 4. LP-R/C@AC. (F) TEM images of LP-R/C@AC in different pH buffer solutions for 48 h, scale bar: 100 nm; (G) AP and CS-1 drug release rate of LP-R/C@A and LP-R/C@C in different pH buffer solutions.

introduction of the red cell membrane increased the distance between the DiI-DiO pair, which was reflected by the recovery of the fluorescence signal of DiI (Fig. S3, ESI†).

By analyzing the overall membrane constituents using the SDS-PAGE method, we found good retention of the characteristic protein inherited from the RBC and HGC-27 membrane in the protein profile of the R/C hybrid membrane and LP-R/C@AC NPs (Fig. 2D). Furthermore, we analyzed the specific protein markers (CD47 for RBC and CD44 for gastric cancer cells) of the R/C hybrid membrane and LP-R/C@AC NPs. CD47 is a glycoprotein acting as a "don't-eat-me" signal.[24] The results showed that CD47 was not only expressed by RBC but also overexpressed in CCM. This result indicates that the HGC-27 membrane might enhance the immunity escaping ability of LP-R/C@AC NPs *in vivo*. Also, CD44 was reported to be highly expressed on gastric cancer cells.[25] Consistent with this point, Fig. 2E also indicated the high expression of CD44 in the HGC-27, hybrid membrane, and LP-R/C@AC NPs. Considering the high expression of hyaluronan (HA) on gastric cancer and the role of CD44 as a HA receptor,[26] we suspect that the presence of the HGC-27

membrane can significantly contribute to the homotypic targeting and tumor homing characteristics of LP-R/C@AC NPs.

We next validated the pH-triggered drug release functionality of LP-R/C@AC NPs using different methods. The TEM images showed that the LP, LP@AC and LP-R/C@AC were spherical NPs (Fig. 2F and Fig. S4, ESI†) in the normal pH conditions (pH 7.4). However, the LP-R/C@AC NPs gradually lost their structure and eventually disassembled at pH 5.2 (Fig. 2F). The morphology change directly resulted in the size increase of LP-R/C@AC NPs, the two-dimensional lamellar membranes at acidic environment. On the contrary, the particle size of the pH-insensitive liposomes remained almost constant (Fig. S5, ESI†). The drug release assay indicated that about 82% AP and 89% CS-1 were released from LP-R/C@AC after 72 h of incubation in acidic condition (PBS, pH 5.2), while only about 44% and 52% of the loaded AP and CS-1 were released at normal condition (PBS, pH 7.4) (Fig. 2G). Considering the pH values between endosomes/lysosomes and the tumor-microenvironment, we speculated that the release rate of the drug at pH 5.2 (endosomes/lysosomes environment) was quicker and more thorough as compared with the relatively low release speed in the slightly acidic tumor micro-environment, which was consistent with a previous report.[17]

Biocompatibility of LP-R/C NPs

Liposomes, which have biocompatible, biodegradable, and nano-scale properties, have become a mainstream nanodrug delivery carrier.[16] By further evaluating the biocompatibility of hybrid membrane-modified pH-responsive liposome drug delivery carriers (LP-R/C NPs) with CCK-8 assay, we found that all the investigated cell survival rates were more than 90%, even at the high concentration of 60 μg mL^{-1} (Fig. 3A), which indicated that these kinds of nanoparticles exhibited low cytotoxicity to both human normal cells (SMC and HUVEC) and cancer cells (HGC-27). Hemolysis assay showed that except for the solo CS-1 group, the hemolysis rates of samples treated with AP, AC, LP@AC and LP-R/C@AC NPs were less than 5%, even at the high concentration of 120 μg mL^{-1}. Consistent with this result, the supernatant was transparent (Fig. 3C). Moreover, a high concentration of unwrapped apatinib (group AP and AC) caused erythrocyte contraction to some extent, and they also led to slight platelet aggregation in the blood (Fig. 3B and D). However, these side effects disappeared after loading them into the hybrid membrane-modified nanocomplex. These data indicated that LP-R/C NPs can significantly improve the biocompatibility of AP and CS-1.

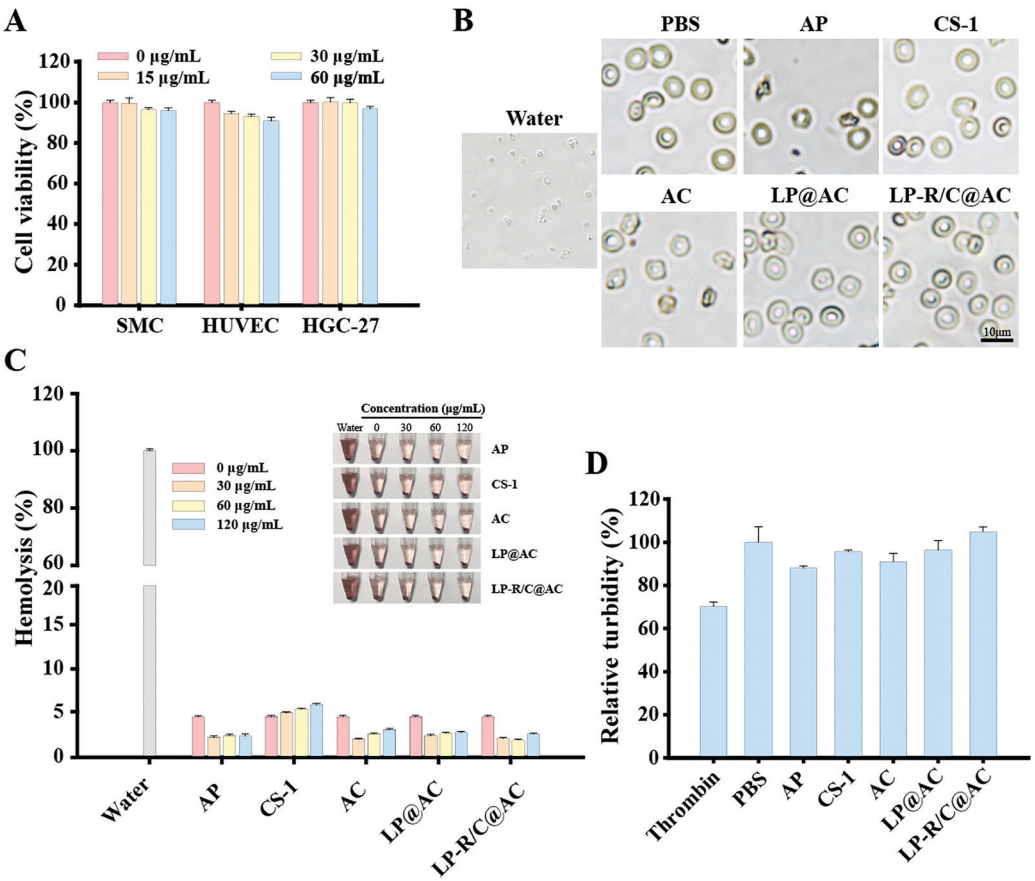

Fig. 3 (A) Biocompatibility of LP-R/C NPs (without loading AP or CS-1) to different cells. Note: When the concentrations of the encapsulated drugs for AP and CS-1 are 10 μM and 30 nM, respectively, the amount of LP-R/C NPs is 15 μg mL^{-1}. (B and C) The images and quantification analysis of hemolysis assay. (D) Platelet aggregation assay of different formulations.

Enhanced tumor cell-killing activity of LP-R/C@AC NPs *in vitro*

By employing the CCK-8 assay to probe the effect of drugs on the tumor cell viability after loading into LP-R/C NPs, we found that the combined utilization of AP and CS-1 still had an outstanding killing effect on tumor cells (Fig. 4A). On the other hand, compared to the unwrapped drug groups (Fig. 1C), the LP-R/C NPs nanocarriers significantly extended the drug release cycle, which could weaken the toxic and side effects of the instantaneously high concentration of the drugs. The live/dead cells staining images in Fig. 4B also demonstrated the excellent killing ability of the AP and CS-1 combined utilization, which is shown by the strongest red signal (dead cells) in the LP-R/C@AC group as compared with other groups.

Previous studies have shown that cinobufagin could exert an anti-proliferative function by inducing ROS.[12] This function was also observed in this study as the ROS (green signal) in HGC-27 cells were significantly increased after treatment with LP-R/C@C NPs and LP-R/C@AC NPs, the two complexes containing CS-1. In contrast, the presence of AP only slightly upregulated ROS (Fig. 4C). The apoptosis assay indicated that

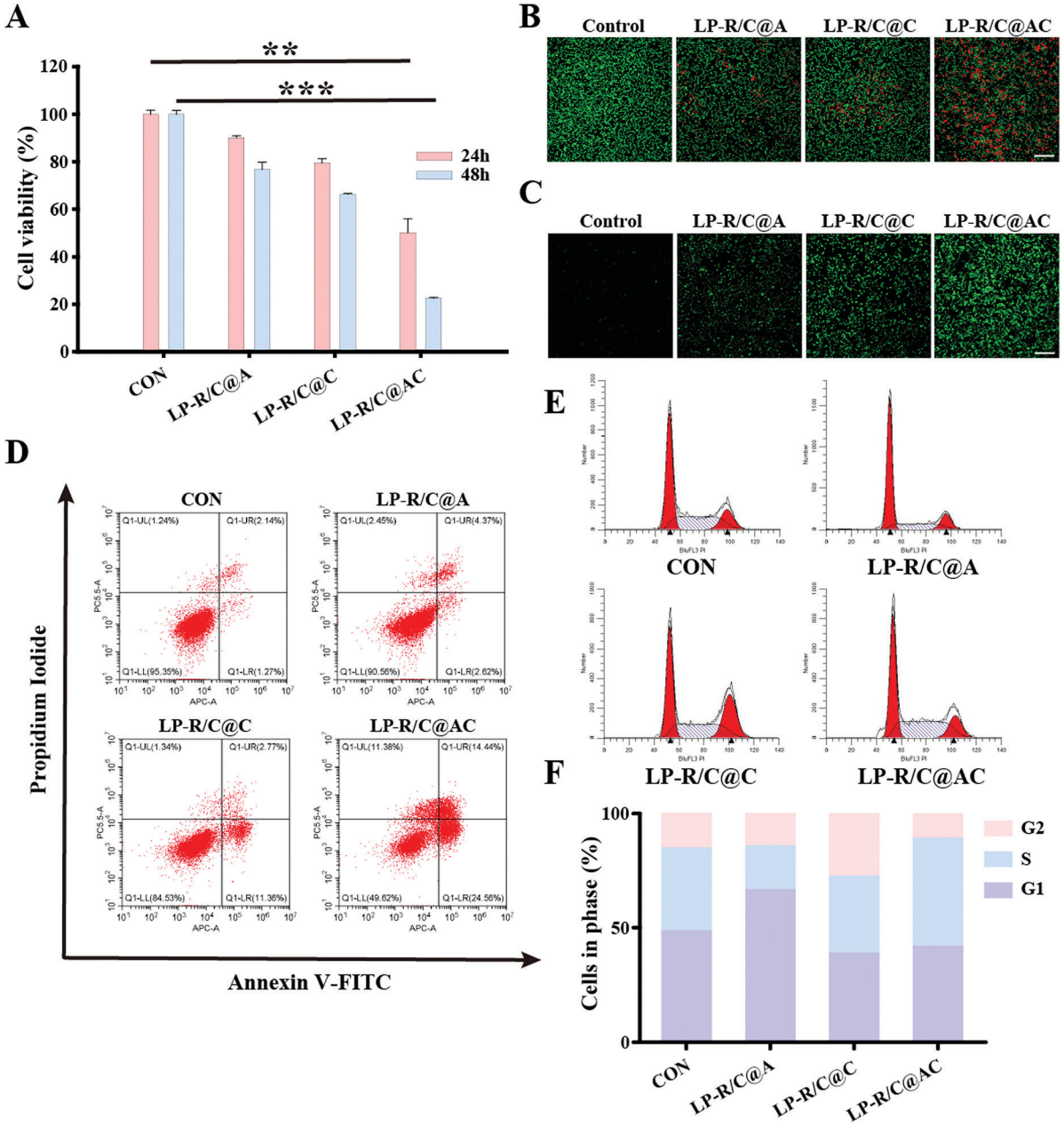

Fig. 4 (A) Cell viabilities of HGC-27 cells by CCK-8 assay after treatment with various formulations. (B) CLSM results of live/dead staining of HGC-27 cells with various treatments for 24 h, scale bar: 200 μm. (C) ROS production of HGC-27 cells with different treatments for 24 h, scale bar: 200 μm. (D) Flow cytometry analysis of HGC-27 cells after treatment with various formulations for 24 h. (E and F) Cell cycle distributions of the HGC-27 cells after incubation with various formulations.

the apoptosis rates of HGC-27 cells were 6.99%, 14.13%, 39.00%, respectively, after treating with LP-R/C@A, LP-R/C@C and LP-R/C@AC NPs (Fig. 4D); the unwrapped drugs (AP, CS-1 and AC) showed similar results (Fig. S6, ESI†). These data confirmed that the combination of these two drugs could significantly increase tumor cell apoptosis as compared with the sole drugs. Moreover, the FACS assay showed that both AP and LP-R/C@A arrested tumor cells cycle in the G1 phase. In contrast, CS-1 and LP-R/C@C arrested tumor cells in the G2 phase. Perhaps, due to the slow release of the two drugs from the nanomaterials, AC treatment arrested cells in the G1 and G2 phases, while LP-R/C@AC arrested tumor cells in the S phase (Fig. 4E, F and Fig. S7, ESI†). These results suggest that LP-R/C@AC can inhibit tumor growth by simultaneously affecting the cell cycle and inducing apoptosis.

In vitro anti-tumor mechanism of LP-R/C@AC NPs

The above molecular docking result indicated that both AP and CS-1 could suppress the function of VEGFR2 by interacting with its amino acid sites. Consistent with this data, both LP-R/C@A and LP-R/C@C treatment inhibited VEGFR2 expression in HGC-27 cells. Moreover, the LP-R/C@AC treatment displayed a stronger inhibitory effect, while the LP-R/C@AC exhibited an excellent inhibitory effect on p-VEGFR2 (Tyr1175) (Fig. 5A and B); this result demonstrated that the combination of AP and CS-1 can enhance the inhibitory effect on this kinase. Accordingly, the levels of the VEGFR2 downstream targets were inhibited. Moreover, the high expression and phosphorylation of STAT3, the downstream molecule of VEGFR2, was reversed by LP-R/C@C and LP-R/C@AC treatment in gastric cancer (Fig. 5A and B), while no effect was found for LP-R/C@A. Consequently, the downstream carcinogenic proteins of STAT3 including HIF-1α, VEGF, PD-L1, Mcl-1 and Cyclin D1 were inhibited (Fig. 5A and B). Compared to the single-drug complexes of LP-R/C@A and LP-R/C@C, the LP-R/C@AC treatment displayed an outstanding tumor inhibition effect due to the multiple functions such as alleviating the hypoxic environment in the tumor site (reduced HIF-1α), decreasing tumor angiogenesis (reduced VEGF), enhancing tumor immunity in the tumor microenvironment (reduced PD-L1), inhibiting tumor cell proliferation (reduced Cyclin D1),[27–29] promoting apoptosis, and reversing the multidrug-resistance (reduced Mcl-1),[30] which make this system an ideal strategy for gastric cancer therapy. Besides, the NF-κB, which plays an essential role in inflammation, innate immunity and cancer progression, was also significantly inhibited by LP-R/C@AC. These results suggest that LP-R/C@AC can inhibit tumors at multiple levels.

Fig. 4D shows that HGC-27 cells can be killed by AP, CS-1 and the combination, by inducing apoptosis. We explored proteins related to cell apoptosis and found that both AP and CS-1 could upregulate Bax, while downregulating the Bcl-2 level. Meanwhile, compared with the control, cleaved Caspase-3 in HGC-27 cells was increased when cells were treated with LP-R/C@A and LP-R/C@C, and the combinational group LP-R/C@AC showed the strongest cleaved Caspase-3 band (Fig. 5A and B). These results indicated that combinational treatment with AP and CS-1 improved apoptosis induction in HCG-27 cells.

Pyroptosis is a mechanism of programmed cell death mediated by the gasdermin family.[31] As a member of the gasdermin family with tumor-suppressing function, DFNA5/GSDME was significantly suppressed or silenced in gastric cancer, while DFNA5 upregulation often leads to the pyroptosis of tumor cells and makes them more sensitive to chemotherapeutic drugs.[32] Fig. 5A and B show that CS-1 significantly upregulated the DFNA5 level, which can make gastric cancer cells more susceptible to AP to achieve a better tumor-killing effect. Pyroptosis triggered by CS-1 could cause the immunological death of tumor cells, which can promote the release of tumor-associated antigens and activate specific anti-tumor immune responses, achieving a systemic tumor treatment effect.

Cinobufagin was reported to induce tumor death through autophagy in U2OS cells.[33] Similarly, CS-1 remarkably increased the ratio of LC3-II/LC3-I in HCG-27 cells (Fig. 5A and B), which is closely related to the activation of autophagic activity; moreover, the combination treatment further increased this ratio. These results indicated that CS-1 could activate ROS-induced autophagy in gastric cancer as well, and the combination with AP could further amplify the tumor cell killing effect.

To explore the underlying molecular mechanisms of cell cycle arrest caused by AP and CS-1, the levels of Cyclin D1 and p21, the most important cell cycle-related proteins, were detected. Regulated by STAT3 and NF-κB,[27,34] Cyclin D1 exerts an important role in regulating cell cycle progression and a variety of tumorigenic processes, while p21 is a cell cycle inhibitor and anti-proliferative effector as tumor suppressor.[35] Fig. 5A and B show that Cyclin D1 decreased in LP-R/C@A, LP-R/C@C and the combinational LP-R/C@AC group, while p21 significantly increased in the LP-R/C@C group and the combinational LP-R/C@AC group. The different expression patterns of the two proteins contributed to cell cycle arrest in different phases.

Anti-migration capability of LP-R/C@AC NPs *in vitro*

Cell migration and invasion are essential for tumor recurrence and metastasis, which are tightly related to STAT3 and HIF-1α.[27,36] The results of the wound healing assay showed that both AP and CS-1 significantly inhibited the migration of HGC-27 cells ($p < 0.0001$), while the combinational treatment exhibited the strongest inhibitory effect. The migration rate of the LP-R/C@AC was only about 1/4 of that of the control group and 1/2 of that of two separate drug groups (Fig. 6A and B). As a metalloproteinase, MMP-9 played an essential role in tissue remodeling by degrading the extracellular matrix (ECM) components, which is essential for tumor invasion and metastasis.[37] Vimentin is a marker for epithelial–mesenchymal transition (EMT), the overexpression of which is associated with the depth of invasion and lymph node metastasis.[38] To explore the anti-migration mechanism of LP-R/C@AC NPs, we detected the levels of the two proteins. As we expected,

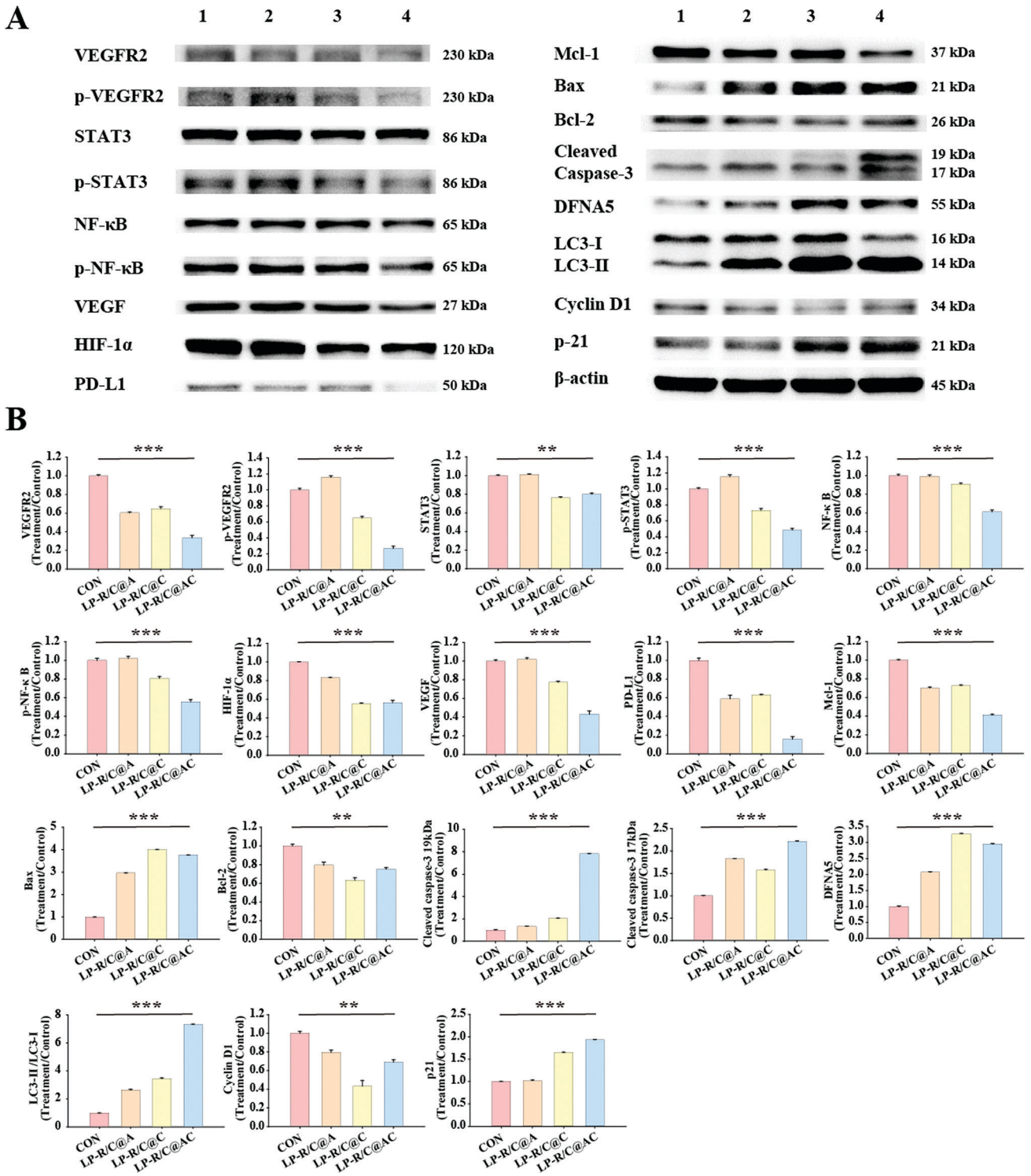

Fig. 5 (A) Western blotting analysis. (B) Quantitative analysis of various proteins after different treatments: 1. CON, 2. LP-R/C@A, 3. LP-R/C@C, 4. LP-R/C@AC.

MMP-9 and vimentin in HGC-27 cells were significantly inhibited after treating with AP or CS-1-containing treatment, and the combinational group showed the strongest inhibitory effect (Fig. 6C and D). Moreover, the immunofluorescence assay also indicated the effective inhibition of vimentin in HGC-27 cells after LP-R/C@AC NPs treatment as compared with the control group (Fig. 6E), which was reflected in the decreased green fluorescence. In addition to these proteins, the cell cycle arrest caused by the drug treatment was helpful for the anti-metastatic effect.

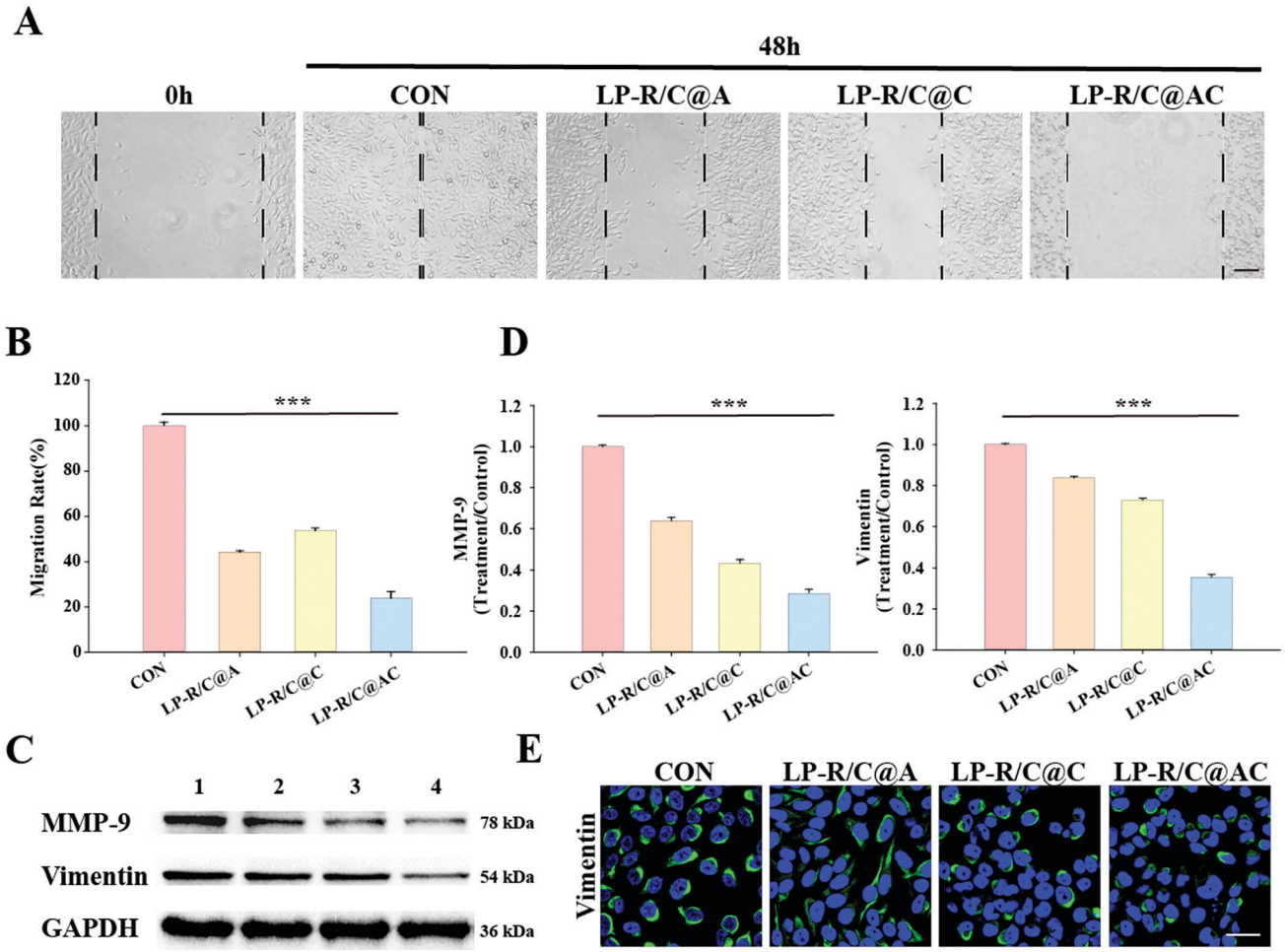

Fig. 6 *In vitro* anti-metastatic ability of AP and CS-1. (A) Wound-healing assay of HGC-27 cells with different treatments, scale bar: 100 μm. (B) Quantitative analysis of the migration rate. (C and D) Western blot assay of MMP-9 and vimentin protein expression levels in HGC-27 cells with various treatments. (E) Immunofluorescence assay of vimentin expression levels in HGC-27 cells with different treatments, scale bar: 30 μm.

Immune escape, tumor targeting and pharmacokinetics of LP-R/C@AC NPs

Red blood cell membranes can efficiently improve immune escape through special surface proteins such as CD47.[39] To study the immune evasion ability of LP-R and LP-R/C NPs, we incubated macrophages with nanomaterials to mimic the *in vitro* immune environment. Fig. 7A shows that the intracellular red fluorescence intensity of LP-R and LP-R/C NPs decreased by 44.3% and 27.5%, as compared with LP NPs, demonstrating that red blood cell membranes camouflage can decrease the uptake by macrophages. The killing efficiency of the nanodrug was directly determined by the internalization into tumor cells; therefore, we explored the internalizing ability of LP-R/C NPs and found the marked augmentation of red fluorescence (14.7-fold) in tumor cells as compared with LP NPs (Fig. 7B) while no significant difference was found in normal cells (Fig. S8, ESI†), which indicated that the tumor cell membranes endow the nanocarriers with strong homologous targeting ability. These results indicate that the LP-R/C NPs possess good immune escape ability and they also effectively enter into cancer cells with the aid of hybrid membrane encapsulation. The uptake mechanism of LP-R/C NPs was investigated and it was found that LP-R/C NPs were taken into tumor cells mainly through macropinocytosis and membrane fusion, which was reflected in the reduced red fluorescence in the Active Ingredient treated group,[40] while the chloroquine and methyl-β-cyclodextrin-treated groups showed no significant changes (Fig. S9, ESI†). Soon after entering into cells, LP-R/C NPs were carried to lysosomes to release drugs under an acid environment (Fig. S9, ESI†).

The pharmacokinetics and biodistribution of nanocarriers by intravenously injecting them into BALB/c mice were examined. As shown in Fig. 7C, the fluorescence intensity of blood samples decreased gradually over time. The half-lives of Cy5.5, LP, and LP-R/C NPs were calculated to be 0.56, 0.94 and 1.97 h, respectively (Fig. 7D). Compared with Cy5.5, the half-time of LP-R/C NPs *in vivo* increased 3.52-fold (0.56 h *vs.* 1.97 h), which demonstrated that the hybrid membrane coating extended the blood retention time of LP-R/C NPs.

By the real-time monitoring of the biodistribution of nanoparticles, LP-R/C NPs were found to gradually accumulate at tumor sites, which was reflected by the Cy5.5 fluorescence

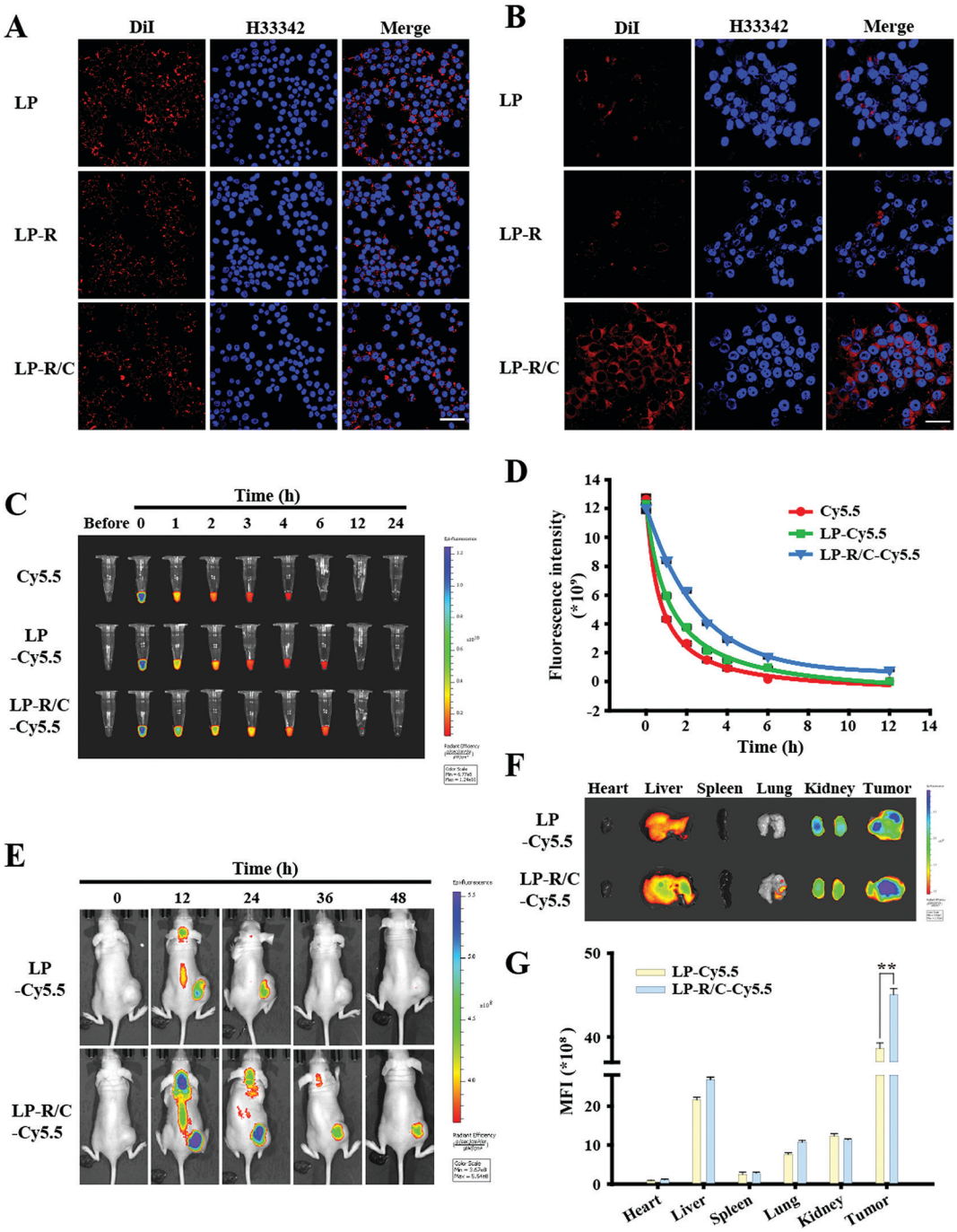

Fig. 7 (A) Immune evasion of LP, LP-R, and LP-R/C NPs, scale bar: 40 μm. (B) Tumor cellular uptake of LP, LP-R, and LP-R/C NPs, scale bar: 40 μm. (C) Concentration of Cy5.5, LP-Cy5.5, and LP-R/C-Cy5.5 NPs in the blood at various time points. (D) Pharmacokinetic curves of Cy5.5, LP-Cy5.5, and LP-R/C-Cy5.5 NPs post-intravenous administration in BALB/c mice. (E) Biodistribution of LP-Cy5 and LP-R/C-Cy5 in HGC-27 tumor-bearing BALB/c nude mice at different time points. (F and G) Relative fluorescence signals and quantitative analysis of major organs.

signal and the signal intensity reached a plateau within 12 h after administration. Moreover, the signal can remain in the tumor tissue for up to 48 h (Fig. 7E). Similarly, sole LP NPs without the membrane coating partly accumulated in the tumor site due to the EPR effect. Also, *ex vivo* images directly indicated the fluorescence difference in mice tumor tissue with LP and LP-R/C NPs treatment. The results indicated that LP-R/C NPs possessed a good affinity for both subcutaneous and metastatic tumor tissues by elongating the blood circulation time and outstanding tumor-targeting ability (Fig. 7F and Fig. S10, ESI†). Moreover, no obvious fluorescence signal was found in the heart and spleen of mice with LP-R/C NPs treatment. This result demonstrated that the membrane coating can effectively alleviate the toxic side effects of CS-1

on the heart. Finally, by studying the metabolic patterns of nanoparticles, LP NPs were found to be metabolized effectively through the liver and kidneys, whereas LP-R/C NPs were mainly metabolized through the liver due to the larger size (Fig. 7G).

Anti-tumor activity of LP-R/C@AC NPs *in vivo*

In consideration of the efficient tumor cell killing ability *in vitro* and the efficient accumulation at the tumor site *in vivo*, we investigated the anti-tumor ability of LP-R/C@AC NPs *in vivo*. Fig. 8A and B show that CS-1 (TIR: 44.88%), AP (TIR: 54.29%), or AC (TIR: 63.79%) treatment partially inhibited the tumor growth of mice, while LP@AC treatment significantly improved the tumor inhibition ability (TIR: 76.82%). Moreover, the tumor growth was almost inhibited after treatment with LP-R/C@AC (TIR: 86.78%). No significant change was found for the body weight of each group (Fig. 8C).

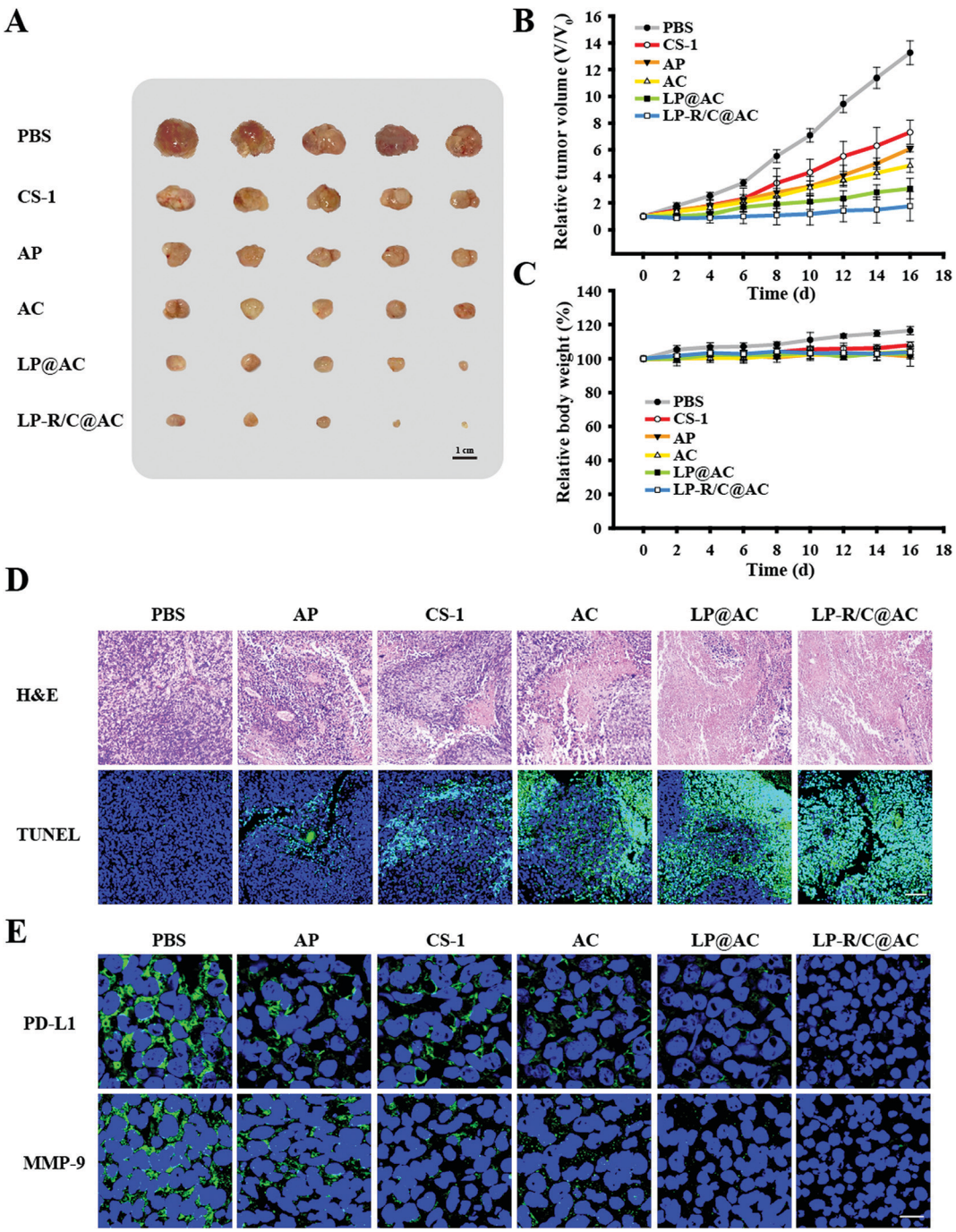

Fig. 8 Antitumor effect of LP-R/C@AC NPs *in vivo*. (A) Images of tumors treated with different formulations. (B) The relative volumes of tumors. (C) Relative body weight of HGC-27 tumor-bearing BALB/c nude mice during chemotherapy (n = 5). (D) H&E and TUNEL for tumor paraffin sections in each group, scale bar: 100 μm. (E) PD-L1 and MMP-9 expression levels of tumor paraffin sections by immunofluorescence, scale bar: 15 μm.

To support these findings, we performed cell death analysis in tumor tissue using H&E staining and TUNEL analysis. Fig. 8D displays the preeminent anti-tumor ability of LP-R/C@AC NPs as compared with other groups. As shown in H&E staining, the control tumor cells showed the complete structure with condensed chromatin and nucleus, while most of the tumor cells with LP-R/C@AC treatment were in apoptotic and necrotic states. Also, large areas with green fluorescence signals

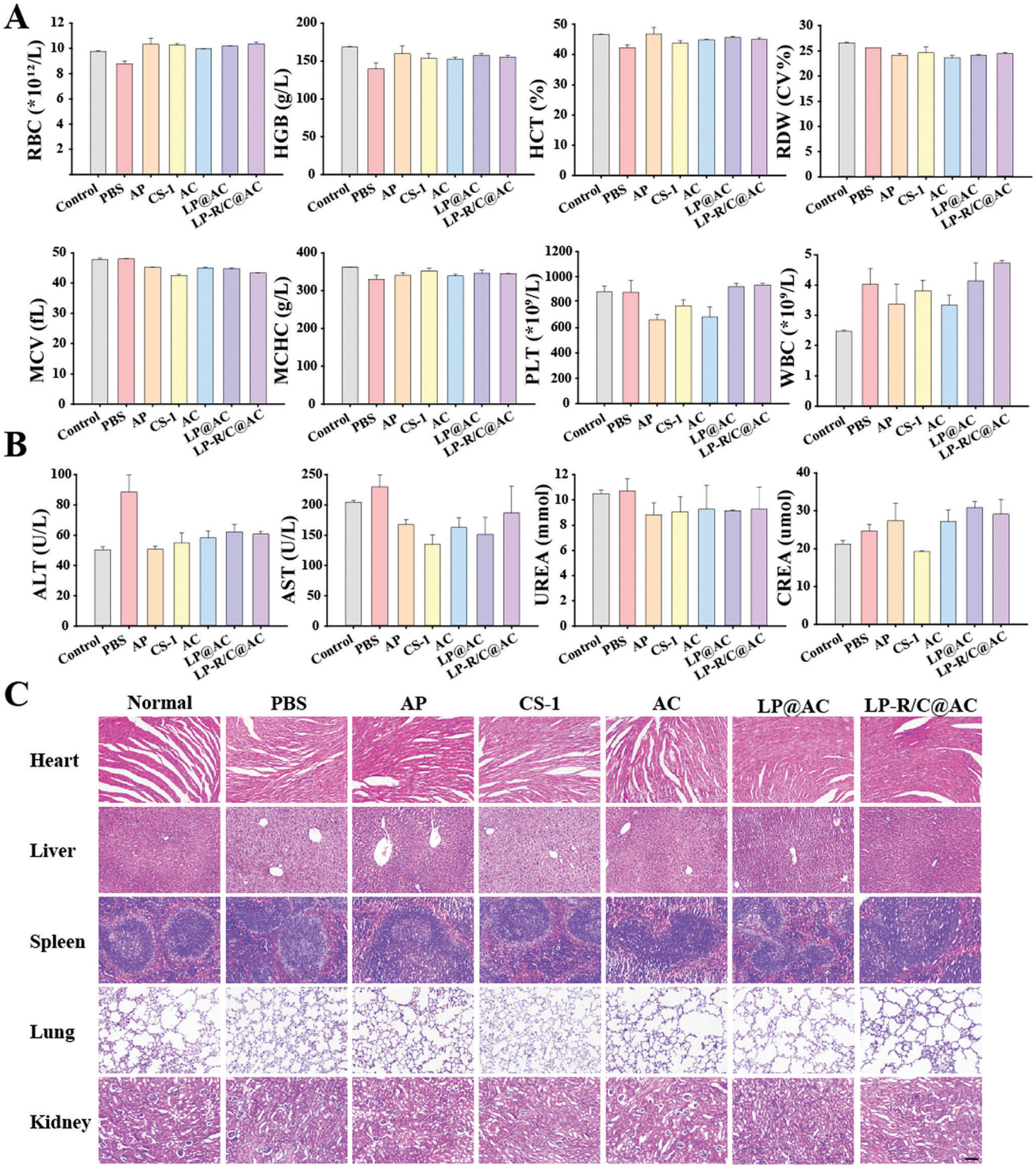

Fig. 9 *In vivo* toxicity evaluation. (A) Complete blood panel analysis. RBC: red blood cell, HGB: hemoglobin, HCT: hematocrit, RDW: red blood cell distribution width, MCV: mean corpuscular volume, MCHC: mean corpuscular hemoglobin concentration, PLT: platelets, WBC: white blood cell. (B) Blood biochemistry data including liver function markers: ALT and AST, and kidney function markers: UREA and CREA. (C) H&E stained slices of major organs.

in LP-R/C@AC treatment tumor tissue indicated massive apoptotic tumor cells and obvious tumor tissue destruction.

Next, an immunofluorescence assay was employed to explore the influence of different treatments on the expression of PD-L1 and MMP-9 *in vivo*. Fig. 8E shows that AP and CS-1 could inhibit the expression of PD-L1 and MMP-9 to a certain degree in tumor tissue, while the combination therapy exhibited the strongest suppression since the green fluorescence could hardly be found in the tumor tissue with LP-R/C@AC treatment. This result suggested that the LP-R/C@AC treatment could inhibit tumor invasion and metastasis to a great extent, relieve the immunosuppression effect in the tumor micro-environment, and greatly stimulate the anti-tumor immune response. Taken together, these findings manifested that the LP-R/C@AC NPs exerted favorable anti-tumor function *in vivo*.

Toxicity evaluation *in vivo*

The toxicity and side effects of LP-R/C@AC NPs *in vivo* were carefully considered using different parameters. First, blood chemistry analysis displayed that the direct administration of drugs (AP, CS-1 and AC) caused damage to the blood system, which is reflected in the reduction of PLT. However, the relevant parameters were still within the normal range when the drugs were loaded in the nanoparticles. *In vivo* administration indicated that the WBC number increased in the mice with the LP-R/C@AC treatment, compared with the tumor-bearing mice in the untreated PBS group, which suggested the down-regulation of tumor immunosuppression-related proteins such as PD-L1 to stimulate the immune response against tumor tissues and achieve a better therapeutic effect (Fig. 9A).

Hepatic and renal function analysis displayed a significant increase in ALT in the tumor-bearing mice treated with PBS, which could be reversed by the LP-R/C@AC treatment in the normal range. The AST, UREA and CERA of the LP-R/C@AC group showed no significant change as compared with healthy mice, which indicated the excellent anti-tumor effect of LP-R/C@AC *in vivo* without obvious toxic/side effects on the liver and kidney (Fig. 9B). Moreover, H&E staining analysis showed the negligible pathological effects of LP-R/C@AC NPs on the main organs (heart, liver, spleen, lung, and kidney) (Fig. 9C). On the whole, these results manifested the considerable biosafety of LP-R/C@AC NPs *in vivo*, which is necessary and critical for potential clinical applications.

Conclusion

In summary, a biomimetic pH-responsive liposome system integrating the dual advantages of immune escape and tumor cell targeting ability was established for the co-delivery of AP and CS-1 (LP-R/C@AC NPs) to realize efficient tumor ablation. The hybrid membrane prolonged the half-life and reduced the toxic and side effects of the sole AP and CS-1. The homologous targeting ability of the tumor cell membrane improved the drug accumulation in both solid and metastatic tumor tissues. *In vitro* studies showed that LP-R/C@AC can efficiently kill tumor cells by inhibiting the VEGFR2/STAT3 signal pathway *via* inducing apoptosis, autophagy and pyroptosis. Moreover, LP-R/C@AC NPs showed excellent tumor ablation, tumor invasion and metastasis inhibition and reversed tumor immunosuppression *in vivo*. Taken together, LP-R/C@AC NPs demonstrated outstanding anti-tumor efficiency *in vitro* and *in vivo*, showing promising prospects for the clinical chemotherapy of malignant gastric cancer.

Conflicts of interest

There are no conflicts of interest to declare.

Acknowledgements

This work was partially supported by the Natural Science Foundation of Hunan Province (2019JJ50859; 2020JJ4005).

References

1 E. Van Cutsem, X. Sagaert, B. Topal, K. Haustermans and H. Prenen, *Lancet*, 2016, **388**, 2654–2664.
2 Y. Y. Choi and J. H. Cheong, *Eur. J. Surg. Oncol.*, 2017, **43**, 856–864.
3 Cancer Genome Atlas Research Network, *Nature*, 2014, **513**, 202–209.
4 A. Rapisarda and G. Melillo, *Adv. Cancer Res.*, 2012, **114**, 237–267.
5 C. H. Heldin, K. Rubin, K. Pietras and A. Ostman, *Nat. Rev. Cancer*, 2004, **4**, 806–813.
6 Y. Wang, Y. Shen, S. Wang, Q. Shen and X. Zhou, *Cancer Lett.*, 2018, **415**, 117–128.
7 S. Tian, H. Quan, C. Xie, H. Guo, F. Lu, Y. Xu, J. Li and L. Lou, *Cancer Sci.*, 2011, **102**, 1374–1380.
8 R. Geng, L. Song, J. Li and L. Zhao, *Expert Opin. Drug Saf.*, 2018, **17**, 1145–1150.
9 J. Ding, X. Chen, Z. Gao, X. Dai, L. Li, C. Xie, H. Jiang, L. Zhang and D. Zhong, *Drug Metab. Dispos.*, 2013, **41**, 1195–1210.
10 C. Zhang, K. Ma and W. Y. Li, *Drug Des., Dev. Ther.*, 2019, **13**, 4075–4090.
11 X. Li, C. Chen, Y. Dai, C. Huang, Q. Han, L. Jing, Y. Ma, Y. Xu, Y. Liu, L. Zhao, J. Wang, X. Sun and X. Yao, *Cancer Sci.*, 2019, **110**, 1724–1734.
12 S. H. Baek, C. Kim, J. H. Lee, D. Nam, J. Lee, S. G. Lee, W. S. Chung, H. J. Jang, S. H. Kim and K. S. Ahn, *Immunopharmacol. Immunotoxicol.*, 2015, **37**, 265–273.
13 J. Q. Yin, L. Wen, L. C. Wu, Z. H. Gao, G. Huang, J. Wang, C. Y. Zou, P. X. Tan, B. C. Yong, Q. Jia and J. N. Shen, *Toxicol. Lett.*, 2013, **218**, 129–136.
14 X. L. Wang, G. H. Zhao, J. Zhang, Q. Y. Shi, W. X. Guo, X. L. Tian, J. Z. Qiu, L. Z. Yin, X. M. Deng and Y. Song, *J. Asian Nat. Prod. Res.*, 2011, **13**, 383–392.
15 B. Liu, W. Wang, J. Fan, Y. Long, F. Xiao, M. Daniyal, C. Tong, Q. Xie, Y. Jian, B. Li, X. Ma and W. Wang, *Biomaterials*, 2019, **217**, 119301.

16 M. Li, C. Du, N. Guo, Y. Teng, X. Meng, H. Sun, S. Li, P. Yu and H. Galons, *Eur. J. Med. Chem.*, 2019, **164**, 640–653.
17 G. Liu, X. Zhao, Y. Zhang, J. Xu, J. Xu, Y. Li, H. Min, J. Shi, Y. Zhao, J. Wei, J. Wang and G. Nie, *Adv. Mater.*, 2019, **31**, e1900795.
18 M. Wu, W. Le, T. Mei, Y. Wang, B. Chen, Z. Liu and C. Xue, *Int. J. Nanomed.*, 2019, **14**, 4431–4448.
19 J. Fan, B. Liu, Y. Long, Z. Wang, C. Tong, W. Wang, P. You and X. Liu, *Acta Biomater.*, 2020, **113**, 554–569.
20 Y. Long, X. Wu, Z. Li, J. Fan, X. Hu and B. Liu, *Biomater. Sci.*, 2020, **8**, 5088–5105.
21 J. Y. Zhu, D. W. Zheng, M. K. Zhang, W. Y. Yu, W. X. Qiu, J. J. Hu, J. Feng and X. Z. Zhang, *Nano Lett.*, 2016, **16**, 5895–5901.
22 Q. Jiang, Y. Liu, R. Guo, X. Yao, S. Sung, Z. Pang and W. Yang, *Biomaterials*, 2019, **192**, 292–308.
23 T. Takahashi, S. Yamaguchi, K. Chida and M. Shibuya, *EMBO J.*, 2001, **20**, 2768–2778.
24 A. N. Barclay and T. K. Van den Berg, *Annu. Rev. Immunol.*, 2014, **32**, 25–50.
25 I. Morath, T. N. Hartmann and V. Orian-Rousseau, *Int. J. Biochem. Cell Biol.*, 2016, **81**, 166–173.
26 R. H. Tammi, A. Kultti, V. M. Kosma, R. Pirinen, P. Auvinen and M. I. Tammi, *Semin. Cancer Biol.*, 2008, **18**, 288–295.
27 K. Banerjee and H. Resat, *Int. J. Cancer*, 2016, **138**, 2570–2578.
28 H. Yu, M. Kortylewski and D. Pardoll, *Nat. Rev. Immunol.*, 2007, **7**, 41–51.
29 J. Chen, C. C. Jiang, L. Jin and X. D. Zhang, *Ann. Oncol.*, 2016, **27**, 409–416.
30 H. Akagi, H. Higuchi, H. Sumimoto, T. Igarashi, A. Kabashima, H. Mizuguchi, M. Izumiya, G. Sakai, M. Adachi, S. Funakoshi, S. Nakamura, Y. Hamamoto, T. Kanai, H. Takaishi, Y. Kawakami and T. Hibi, *Gastric Cancer*, 2013, **16**, 100–110.
31 C. Rogers, T. Fernandes-Alnemri, L. Mayes, D. Alnemri, G. Cingolani and E. S. Alnemri, *Nat. Commun.*, 2017, **8**, 14128.
32 X. Xia, X. Wang, Z. Cheng, W. Qin, L. Lei, J. Jiang and J. Hu, *Cell Death Dis.*, 2019, **10**, 650.
33 K. Ma, C. Zhang, M. Y. Huang, W. Y. Li and G. Q. Hu, *Oncol. Rep.*, 2016, **36**, 90–98.
34 E. A. Musgrove, C. E. Caldon, J. Barraclough, A. Stone and R. L. Sutherland, *Nat. Rev. Cancer*, 2011, **11**, 558–572.
35 B. Shamloo and S. Usluer, *Cancers*, 2019, **11**, 1178.
36 S. Unwith, H. Zhao, L. Hennah and D. Ma, *Int. J. Cancer*, 2015, **136**, 2491–2503.
37 S. Mondal, N. Adhikari, S. Banerjee, S. A. Amin and T. Jha, *Eur. J. Med. Chem.*, 2020, **194**, 112260.
38 A. Satelli and S. Li, *Cell. Mol. Life Sci.*, 2011, **68**, 3033–3046.
39 L. He, T. Nie, X. Xia, T. Liu, Y. Huang, X. Wang and T. Chen, *Adv. Funct. Mater.*, 2019, **29**, 1901240.
40 J. Conde, N. Oliva, M. Atilano, H. S. Song and N. Artzi, *Nat. Mater.*, 2016, **15**, 353–363.